RESEARCH ARTICLE

Check for updates

Integrated proteomic and metabolomic profiling of urine of renal anemia patients uncovers the molecular mechanisms of roxadustat†

Xiaoe You, [ID] ‡[a] Baochun Guo,‡[abc] Zhen Wang,[abc] Hualin Ma,[abc] Lixia Liu,[abc] Ru Zhou,[abc] Yaxuan Zheng[a] and Xinzhou Zhang*[abc]

Roxadustat (FG-4592) is a hypoxia-inducible factor prolyl hydroxylase inhibitor (HIF-PHI) prescribed to patients with low hemoglobin associated with chronic kidney disease. Due to the various HIF-mediated adaptive responses, FG-4592 has attracted significant interest for therapeutic use against various diseases. However, the clinical application of Roxadustat remains limited due to a lack of understanding of its underlying mechanisms. Herein, we performed label-free quantitative liquid chromatography with tandem mass spectrometry (LC-MS–MS) proteomics and un-targeted metabolomics to study the protein and metabolite alterations in the urine of renal anemia patients before and after Roxadustat therapy. The results were validated by parallel reaction monitoring (PRM). A total of 46 proteins (including 15 upregulated and 31 downregulated proteins) and 207 metabolites were significantly altered after Roxadustat treatment in urine samples obtained from renal anemia patients. Then, the altered proteins were further validated by PRM. Finally, proteomics combined with metabolomics analysis revealed that the Ras signalling pathway, cysteine and methionine metabolism, arginine and proline metabolism, and cholesterol metabolism were the main pathways altered by Roxadustat treatment. The multi-omics analysis revealed that Roxadustat could alter the protein expression and reverse the potential metabolic changes to exert hypotensive, lipid metabolic regulation, and renoprotective effects in clinical practice.

[a] *The Second Clinical Medical College, Jinan University (Shenzhen People's Hospital), Shenzhen 518020, Guangdong, China. E-mail: xin.zhou2@qq.com*
[b] *Department of Nephrology, Shenzhen Peoples Hospital (The Second Clinical Medical College, Jinan University, The First Affiliated Hospital, Southern University of Science and Technology), Shenzhen 518020, Guangdong, China*
[c] *Shenzhen Key Laboratory of Kidney Diseases, Shenzhen People's Hospital (The Second Clinical Medical College, Jinan University, The First Affiliated Hospital, Southern University of Science and Technology), Shenzhen 518055, Guangdong, China*

† Electronic supplementary information (ESI) available: Supplementary file 1: List of total proteins in urine between CKD patients before and after Roxadustat treatment. Supplementary file 2: Table comparing the DEPs verified by PRM assay and label-free quantitative proteomics analysis. Supplementary file 3: List of total metabolites in urine between CKD patients before and after Roxadustat treatment. Supplementary file 4: The correlation between differential protein expression and metabolite levels was visualized in a heatmap. The horizontal axis is the clustering of differential proteins, and the vertical axis is the clustering of differential metabolites. Supplementary file 5: Co-expression network of differential proteins and metabolites. The blue circle is the metabolite, and the red circle is the protein. The green line indicates that there is a negative regulatory relationship, and the orange line indicates that there is a positive regulatory relationship between protein and metabolite. The size of the circle indicates the degree of the protein or metabolite in the network (the regulatory efficiency was represented by the size of the nodes). See DOI: https://doi.org/10.1039/d3mo00015j

‡ Xiaoe You and Baochun Guo contributed equally to this work and share the first authorship.

1 Introduction

Roxadustat is a specific hypoxia-inducible factor prolyl hydroxylase inhibitor (HIF-PHI) that has been approved for renal anemia treatment in dialysis and non-dialysis patients mediated by inhibiting the activity of prolyl hydroxylase domain (PHD) protein under normoxic conditions, which in turn, lead to the stabilization of hypoxia-inducible factors (HIF).[1] It has been shown that HIF regulates the expression of erythropoietin (EPO), hepcidin, and other associated factors to promote erythropoiesis at multiple levels.[2] Roxadustat has been widely used in clinical practice due to its advantages, including safety and clinical curative effect.[3] Moreover, it is widely thought that this agent may have consequences beyond correcting renal anemia owing to the variety of HIF-regulated adaptive responses.[4] There is an increasing consensus that Roxadustat is a promising candidate for treating a variety of diseases beyond anemia,[5] including hyperlipidemia,[6,7] kidney injury,[8] and hypertension.[9]

Roxadustat has been identified as a promising therapeutic drug used for dyslipidemia in many randomized controlled trials (RCTs). In this respect, during a phase 3 trial conducted at 29 sites in China, the reduction from baseline in the total

cholesterol level was 40.6 mg per deciliter after Roxadustat treatment and 7.7 mg per deciliter in the placebo group.[10] Wu et al. demonstrated that the Roxadustat treatment group decreased the total cholesterol and LDL levels compared with the placebo group. Back in 2007, it was reported that HIF mediated an increase in the amount of Insig-1 and Insig-2, which accelerated the degradation of 3-hydroxy-3-methyl-glutaryl-CoA reductase, and finally slowed down the rate-determining step of cholesterol synthesis,[11] suggesting a potential role for Roxadustat in serum lipid metabolism, although the underlying mechanism remains unknown.

The reno-protective effect of Roxadustat has been verified via in vitro and in vivo experiments. A huge number of independent studies have demonstrated that Roxadustat can act as a potential therapeutic agent for different types of acute kidney injury (AKI) in humans by potential mechanisms that are involved in diminishing tubular epithelial cell (TEC) injury, suppressing sequence inflammatory responses, etc.[8,12–14] At the same time, Roxadustat can reportedly delay the AKI to chronic kidney disease (CKD) transition by improving vascular regeneration and anti-oxidative capabilities.[15] Notwithstanding that previous studies have demonstrated the roles of Roxadustat on AKI, it remains unclear whether similar protective roles against CKD exist, warranting further exploration.

Long-term high blood pressure is one of the major risks for CKD pathogenesis. A previous study demonstrated that conditional deletion of HIF1α in mice models from vascular smooth muscle cells (VSMCs) enhanced the systolic, diastolic, and mean arterial pressure (MAP) of mice.[16] Jing Yu et al. demonstrated that systemic administration of the HIFα stabilizer FG-4592 reversed the hypertension phenotype and organ injury induced by angiotensin II (Ang II) by enhancing endothelial NO synthase (eNOS) and differentially regulating angiotensin receptor type 1 (AGTR1) and AGTR2 in the vasculature.[9] Besides, overexpression of HIF2α exacerbating pulmonary hypertension has been reported.[17,18] Even though the correlation between Roxadustat and HIF in blood pressure has been established, the interplay and mechanisms among Roxadustat, HIF, blood pressure regulation, and associated networks warrant further investigation. At the same time, most studies as mentioned above are focused on a preclinical trail without a detailed mechanistic demonstration, and it will be necessary to digest the deep molecular event of Roxadustat at multiple levels using different models.

Proteomics and metabolomics are popular platforms used for clinical diagnosis and therapeutics-target screening, which have been extensively utilized in identifying diagnostic biomarkers and exploring the pathophysiological mechanisms of various diseases.[19] Proteomics has been mainly used to identify significantly altered proteins in biological tissue, while metabolomics refers to the comprehensive and quantitative analysis of all metabolites in complex biochemical mixtures, characterizing biological systems. Meanwhile, mass spectrometry (MS)-based proteomics and metabolomics are powerful technologies that are widely applied in molecular biology.

Urine is derived from peripheral circulation and is a more accessible source for diagnosing several diseases, especially kidney disease.[20–22] Herein we employed label-free quantitative proteomic and non-targeted metabolomic methods to investigate the molecular alterations in urine obtained from renal anemia patients that receive Roxadustat treatment. Parallel reaction monitoring (PRM) further validated the significantly altered proteins. By co-analysing the proteomics and metabolomics data, we further revealed the regulatory network involved in these two approaches. To our knowledge, this is the first report utilizing a multi-omics approach to investigate the global response of urine proteins and urine metabolites in renal anemia due to Roxadustat treatment. Importantly, our findings provide new insights into understanding the potential mechanism of Roxadustat during clinical practice.

2 Materials and methods

2.1 Patient assessments and sample collection

12 urine samples were retrieved from 6 patients with renal anemia at the Shenzhen People's Hospital. Patients with anemia due to other causes or severe comorbidities, such as cardiovascular, anaphylactoid purpura, liver diseases, urinary tract infection, and serious gynecological disorders, were excluded. The study was conducted in accordance with the principles of the Declaration of Helsinki and approved by the Ethics Committee of the Second Clinical Medical College (Shenzhen People's Hospital) of Jinan University. All subjects provided informed consent.

The urine samples (50 mL for each patient before and after 1 month of medication, 6 patients in total) were centrifuged at 4 °C for approximately 10 min at $1000g$ (Centrifuge 5427 R, Eppendorf), and the supernatant was transferred to new tubes and stored at -80 °C. At the same time, details on the clinical characteristics of patients were collected.

2.2 Proteomics analysis

2.2.1 Protein extraction. Samples were removed from -80 °C storage and melted on ice. Then 1.933 mL of mixed urine samples were placed in new 5 mL centrifuge tubes one by one. 67 μL Tris–HCl (pH 8.0, 1.5 M) was added to all samples to a final concentration of 50 mM. Then, the supernatant was removed following centrifugation at $1000 \times g$ for 5 min. The supernatant was collected after centrifugation ($17\,000 \times g$, 4 °C) for 10 min and, after an equal volume (2 mL) of methanol and a 1/4 volume (0.5 mL) of chloroform were added, was vortexed vigorously for 15 s and placed at room temperature for 5 min. After centrifugation at $12\,000 \times g$ for 10 min, the supernatant was discarded, then an equal volume (2 mL) of methanol was added and shaken for 15 sec. The previous step was repeated, and 80 μL lysate (containing 1% SDC) was added. Finally, the protein concentration was quantified using a BCA kit (Beyotime, P0010) according to the manufacturer's instructions.

2.2.2 Trypsin digestion. 100 μg of each sample was taken for enzymatic digestion, and the volume of each sample was adjusted with lysis buffer. The lysed protein solution was reduced with 5 mM dithiothreitol for 30 min at 56 °C. Then the protein

solution was alkylated with 11 mM iodoacetamide for 15 min at room temperature in darkness. Finally, sequencing grade trypsin (Yaxin Bio, cat SRT0201) was added at a 1 : 50 trypsin-to-protein mass ratio for the first digestion overnight and a 1 : 100 trypsin-to-protein mass ratio for a second 4 h-digestion. After the second 4 h enzymatic hydrolysis, the reaction was terminated by adding 10% trifluoroacetic acid (TFA) solution and adjusting the pH to 2–3. Then, the peptides were desalted by solid phase extraction (SPE strata-X, Phenomenex, 8B-S100-AAK). The desalted peptides were dried by vacuum centrifuging and dissolved by mass spectrometry mobile phase A. The sample injection volume was 3 μL.

2.2.3 LC-MS/MS analysis. The digested peptides were dissolved by liquid chromatography and separated using an EASY-nLC 1200 HPLC system (packed with 1.9 μm/120 Å ReproSil-PurC18 resins (Dr Maisch GmbH, Ammerbuch, Germany)). Mobile phase A consisted of 0.1% formic acid and 2% acetonitrile. Mobile phase B consisted of 0.1% formic acid in 90% acetonitrile. The liquid phase gradient was set as follows: 0–68 min, 4–20%B; 68–82 min, 20–32%B; 82–86 min, 32–80%B; 86–90 min, 80%B. The flow rate used was 500 mL min^{-1}. The peptides were injected into the NSI source for ionization and then analysed using an Orbitrap Exploris™ 480 mass spectrometer (Thermo). The voltage settings of the ion source were 2.3 kV, and the FAIMS compensation voltage was set to −45 V and −70 V. Orbitrap was used to detect and analyse the peptide parent ions and their secondary fragments. The first-order mass scans were performed with 60 000 resolutions, and the m/z range for the MS scans was 400–1200. The secondary mass spectrometry scan range had a fixed starting point of 110 m/z, and the secondary scan resolution was set to 30 000. TurboTMT was set to Off. The data acquisition mode was based on the data-dependent scan (DDA) mode. To improve the effective utilization of the mass spectrum, the automatic gain control (AGC) was set at 75%, then the signal threshold was set to 10 000 ions per s, and the maximum injection time was set to 100 ms with 30.0 s dynamic exclusion.

2.2.4 Database search. Secondary ion mass spectrometry data were retrieved using Proteome Discoverer (v2.4.1.15) against the Homo_sapiens_9606_PR_20210721.fasta (78120 sequences), and the anti-library was added to calculate the false-positive rate (false discovery rate [FDR]); the digestion method was set to trypsin (Full); the number of missed cleavages was set to 2; The minimum peptide length was set to 6 amino acids; the tolerance values of the mass error for the primary precursor ion was set to 10 ppm, and the error tolerance of the mass of the second fragment ion was set to 0.02 Da; Carbamidomethyl cysteine (C) was set as a fixed modification and Oxidation (M), Acetyl (N-terminus), Met-loss (M), Met-loss + acetyl (M), and Deamidated (N, Q) as variable modifications. The FDR for the protein identification and peptide-spectrum matches identification was adjusted to 1%.

2.2.5 Bioinformatics methods. Gene Ontology (GO) annotation of the proteome was derived from the UniProt-GOA database (https://www.ebi.ac.uk/GOA/). Proteins underwent GO annotation based on three categories: molecular function,

biological process, and cellular component. The protein domain functional descriptions identified in this study were annotated by InterProScan, which analyzes the data through the InterPro domain database (https://www.ebi.ac.uk/interpro/) and protein sequence alignment. Function enrichment analysis was performed using the Kyoto Encyclopedia of Genes and Genomes (KEGG) pathway (KEGG protein database: https://www.kegg.jp/kegg/pathway.html). The KEGG database was used in this study to identify enriched pathways and to test the enrichment of the different proteins against all identified proteins using a two-tailed Fisher's exact test. The pathways with corrected P values < 0.05 were considered significant and were separated into individual categories. All differentially expressed protein accession numbers or sequences were examined thoroughly by the STRING database (version 10.5) for visualization in a protein–protein interaction network.

2.2.6 Parallel reaction monitoring analysis. Preparations were conducted at the initiation of PRM analysis, including protein extraction and trypsin digestion described in previous procedures. A multi-step gradient was applied with a linear increase from 6 to 20% solvent B in the first 40 min, 20% to 30% in the next 40 to 52 min and a rise to 80% from 52 to 56 min, with a constant flow rate of 500 mL min^{-1} applied for 56 to 60 min on an EASY-nLC 1000 UPLC system. Afterward, the peptides were analyzed by MS/MS in Q Exactive™ Plus (Thermo Fisher Scientific (USA)), combined and connected to the UPLC, then went through the NSI source with the electrospray voltage preset at 2.1 kV. The range of the m/z scan was adjusted from 335 to 1245 for a full scan, and the resulting peptides were detected by Orbitrap at a resolution setting of 17 500. Data were acquired using the data-independent acquisition (DIA) mode. For HCD, the normalized collision energy was set to 28. The automatic gain control (AGC) was set at 3E6 mode for the whole MS, and 5E4 mode was specified for MS/MS. The maximum IT was set at 50 milliseconds for full MS and 142 ms for MS/MS. The isolation window was set to 2.0 m/z for MS/MS. The resulting MS data were processed using Skyline (v.21.1). The peptide settings were as follows: the enzyme was set to Trypsin [KR/P], the maximum missed cleavage was set to 0, the peptide length was set to 7–25, and cysteine alkylation was set as a fixed modification. Transition settings: precursor charges were set as 2, 3, ion charges were set as 1, and ion types were set as b, y. The product ions ranged from ion 3 to the last ion, and the ion match tolerance was set as 0.02 Da.

2.3 Metabolomics analysis

2.3.1 Sample preparation. After thawing at 4 °C, the sample was vortexed for 1 min and mixed evenly. Then, 100 ul/sample urine was transferred into a 2 mL centrifuge tube, and 2-amino-3-(2-chloro-phenyl)-propionic acid (4 ppm) solution prepared with 80% methanol-water 1 : 1 (stored at 20 °C) was added and vortexed for 1 min. Finally, after centrifugation for 10 min at 12 000 rpm and 4 °C, the supernatant was filtered with a 0.22 μm membrane and transferred into the detection bottle for LC-MS detection. A high speed freezing centrifuge was obtained from Hunan Xiangyi Experi ment Equipment Co., Ltd (Hunan, China).

A vortex mixer was obtained from Haimen Kylin-bell Lab Instruments Co., Ltd. (Haimen, China). Microporous membrane filters (0.22 pim) were purchased from Tianjin Jinteng Experiment Equipment Co., Ltd (Tianjin, China). LC-MS grade methanol (MeOH) was purchased from Fisher Scientific (Loughborough, UK). 2-Amino-3-(2-chloro-phenyl)-propionic acid was obtained from Aladdin (Shanghai, China). Ultrapure water was generated using a Milli-Q system (Millipore, Bedford, USA).

2.3.2 LC–MC analysis. Liquid chromatography conditions: The LC analysis was performed on an Ultimate 3000 UHPLC System (Thermo Fisher Scientific, USA). Chromatography was carried out with an ACQUITY UPLC®HSS T3 (150 × 2.1 mm, 1.8 μm) (Waters, Milford, MA, USA). The column was maintained at 40 °C. The flow rate and injection volume were set at 0.25 mL min^{-1} and 2 μL, respectively. For LC-ESI (+)-MS analysis, the mobile phases consisted of (C) 0.1% formic acid in acetonitrile (v/v) and (D) 0.1% formic acid in water (v/v). Separation was conducted under the following gradient: 0–1 min, 2% C; 1–9 min, 2–50% C; 9–12 min, 50–98% C; 12–13.5 min, 98% C; 13.5–14 min, 98–2% C; 14–20 min, 2% C. For LC-ESI (−)-MS analysis, the analytes were carried out with (A) acetonitrile and (B) ammonium formats (5 mM). Separation was conducted under the following gradient: 0–1 min, 2% A; 1–9 min, 2–50% A; 9–12 min, 50–98% A; 12–13.5 min, 98% A; 13.5–14 min, 98–2% A; 14–17 min, 2% A.[23]

Mass spectrum conditions: Mass spectrometric detection of metabolites was performed on Q Exactive (Thermo Fisher Scientific, USA) with an ESI ion source. Simultaneous MS1 and MS/MS (Full MS-ddMS2 mode, data-dependent MS/MS) acquisition was used. The parameters were as follows: sheath gas pressure, 30 arb; aux gas flow, 10 arb; spray voltage, 3.50 kV and −2.50 kV for ESI(+) and ESI(−), respectively; capillary temperature, 325 °C; MS1 range, m/z 81–1000; MS1 resolving power, 70 000 FWHM; number of data dependent scans per cycle, 10; MS/MS resolving power, 17 500 FWHM; normalized collision energy, 30%; dynamic exclusion time, automatic.[24]

2.3.3 Data processing and multivariate analysis. The raw data were first converted to mzXML format by MS Convert in the Proteo Wizard software package (v3.0.8789) and processed using XCMS for feature detection, retention time correction and alignment. The metabolites were identified by mass accuracy (< 30 ppm) and MS/MS data which were matched with HMDB (https://www.hmdb.ca), MassBank (https://www.massbank.jp/), Lipid Maps (https://www.lipidmaps.org), mzCloud (https://www.mzcloud.org) and KEGG (https://www.genome.jp/kegg/). The robust LOESS signal correction (QC-RLSC) was applied for data normalization to correct any systematic bias. After normalization, only ion peaks with relative standard deviations (RSDs) less than 30% in QC were kept ensuring appropriate metabolite identification. The ropls R package was used for all multivariate data analyses and modeling. After scaling the data, models were built on principal component analysis (PCA), orthogonal partial least-square discriminant analysis (PLS-DA) and orthogonal partial least-square discriminant analysis (OPLS-DA). The metabolic profiles were visualized as score plots, where each point represents a sample. The corresponding loading plot and S-plot were generated to provide information on the metabolites that influence the clustering of the samples. All the models evaluated were tested for overfitting with methods of permutation tests. OPLS-DA allowed the determination of discriminating metabolites using the variable importance on projection (VIP). The P value, VIP produced by OPLS-DA, and fold change (FC) were applied to identify significant variables for classification. Finally, P values < 0.05 and VIP values > 1 were used as the threshold criteria for identifying statistically significant metabolites.

2.3.4 Pathway analysis. Differential metabolites were subjected to pathway analysis by MetaboAnalyst, which combines results from powerful pathway enrichment analysis with the pathway topology analysis. The identified metabolites in metabolomics were then mapped to the KEGG pathway for biological interpretation of higher-level systemic functions. The metabolites and corresponding pathways were visualized using the KEGG Mapper tool.

2.4 Integrated analysis of metabolomics and proteomics

We conducted proteomic and metabolomic association analyses for the CKD patients before and after Roxadustat treatment. We calculated all proteins and differentially expressed metabolites and compared their correlations by Spearman rank to analyse the differently expressed metabolites and proteins. Meanwhile, we screened the significantly related differential proteins and metabolites with a Spearman correlation coefficient threshold of > 0.8 and generated a co-expression network using Cytoscape software.

2.5 Statistical analysis

SPSS17.0 software was used for data processing and analysis. The measurement data were expressed as mean ± standard error of the mean (SEM). A paired-sample t-test was used for the characteristics of the samples between the two groups. A P-value < 0.05 was statistically significant.

3 Result

3.1 Participant characteristics and changes in the biochemical indicators

As stated previously, 6 patients with renal anemia treated with Roxadustat were included in this study. The clinical characteristics of these patients are described in Table 1. We found that Roxadustat significantly increased the mean hemoglobin levels (82.67 vs. 90.67 g dl^{-1}, P = 0.05), further validating the effect of FG-4592 on renal anemia. Meanwhile, improvement in lipids demonstrated the potential lipid-lowering effects of Roxadustat. However, there were no significant differences in serum creatinine or the estimated glomerular filtration rate before and after therapy, which may be due to the dynamic changes in serum creatinine and may be controlled by various factors. Patients with renal anemia often have other comorbidities which confer a particularly high risk of CKD progression. No significant change in patient blood pressure was observed

Table 1 Participant characteristics of 6 CKD patients

	Before treatment	After treatment	P value
Demographics			
Age (mean ± SD)	49.67 ± 18.82	49.67 ± 18.82	—
Gender (male/female)	1/5	1/5	
Physical exam			
Hemoglobin (g l^{-1})	82.67 ± 12.04	90.67 ± 15.80	0.05
Low-density lipoprotein (mmol l^{-1})	2.12 ± 0.53	1.45 ± 0.57	0.02
Triglycerides (mmol l^{-1})	2.44 ± 1.66	1.78 ± 1.6	0.10
Total cholesterol (mmol l^{-1})	3.91 ± 0.56	2.66 ± 0.45	0.07
Serum creatinine (SCr)	636.07 ± 322.13	622.61 ± 232.92	0.924

(data not shown), which might be explained by the routine clinical administration of angiotensin-converting enzyme inhibitor (ACEI) or angiotensin receptor blocker (ARB) drugs in CKD patients. Furthermore, the low number of participants and the short follow-up period are non-negligible factors.

3.2 Effect of roxadustat on the urine proteomics of patients

3.2.1 Protein identification. Label-free quantification and LC-MS/MS were applied to analyse the urine proteomic profiles of CKD patients before and after Roxadustat treatment. The quality control test result of the MS data satisfied the experimental requirements: most peptides ranged from 7 to 20 amino acids in length, consistent with the basic principle of trypsin digestion, and more than two unique peptides were considered for each protein quantitation. During our experiment, a total of 1862 proteins were identified in the urine sample of the two groups with FDR < 1%, 1062 of which were further quantified. According to the criteria fold change > 1.2 and P < 0.05, 46 differentially expressed proteins (DEPs) were identified, including 15 upregulated proteins and 31 downregulated proteins, compared with before administration (ESI†). Based on the above data, we performed a systematic bioinformatic analysis of proteins.

3.2.2 Analysis and validation of the DEPs. The DEPs were categorized according to the GO classes: cellular components, molecular function, and biological process (Fig. 1). Significantly enriched GO terms associated with cellular components (Fig. 1B) included extracellular, cell surface, side of the membrane, and external side of the plasma membrane. For the molecular function category (Fig. 1A), immunoglobulin receptor binding,
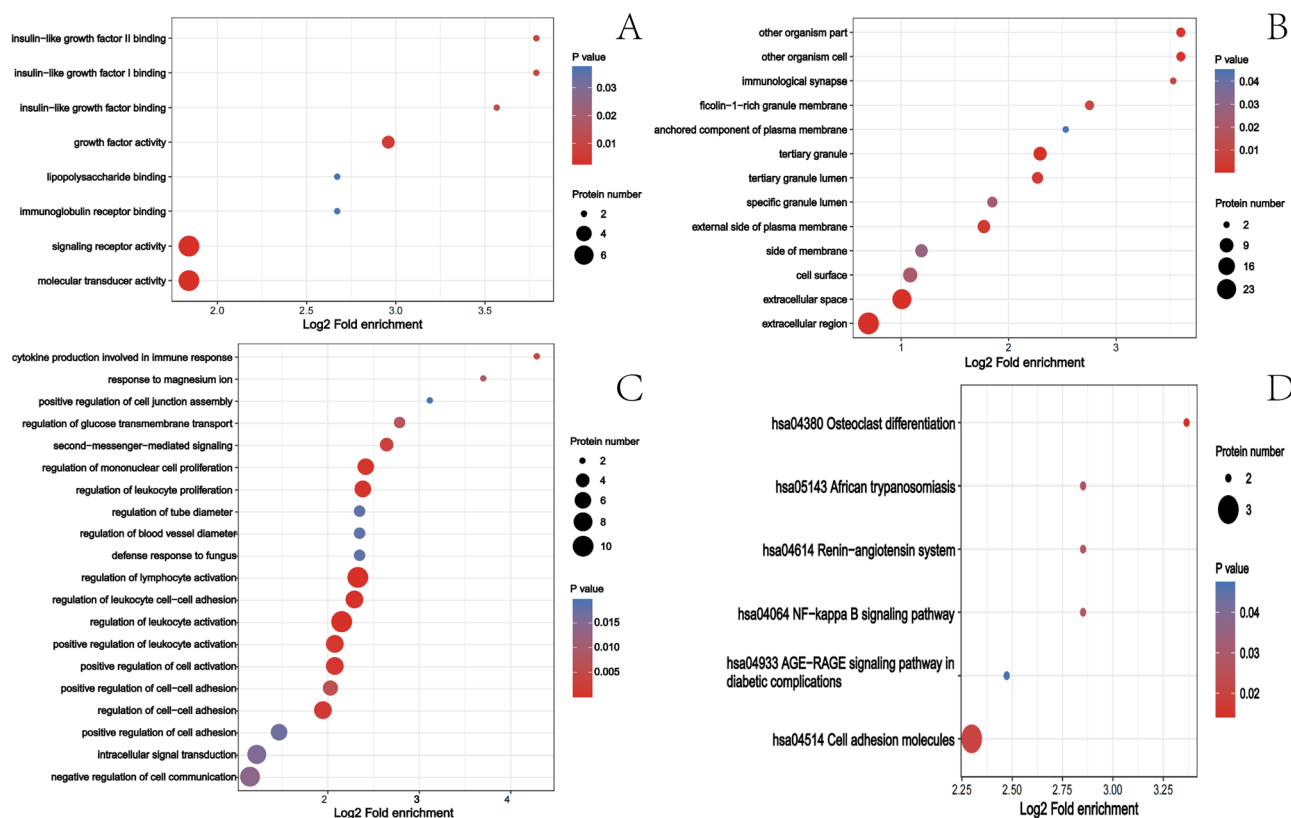

Fig. 1 GO and KEGG analysis of the differential expression of proteins. (A) Molecular function of DEPs. (B) Cellular component of DEPs. (C) Biological process of DEPs. (D) KEGG pathway.

insulin−like growth factor binding, insulin−like growth factor I binding, and insulin−like growth factor II binding were significantly enriched. For the biological process (Fig. 1C), the regulation of leukocyte activation and proliferation, regulation of blood vessel diameter, and regulation of glucose transmembrane transport were significantly enriched. Moreover, KEGG analysis was conducted for functional enrichment analysis of these identified proteins (Fig. 1D). Among these, the AGE-RAGE signalling pathway (hsa04933) in diabetic complications and the Renin−angiotensin system (hsa04614) attracted our attention. Finally, we confirmed that LTF, CHGA, and RARRES2 were upregulated, and LRG1, PI16, and VMO1 were downregulated, consistent with PRM findings. As shown in ESI,† the change in expression of these proteins during PRM analysis was consistent with the label-free proteomics results. However, changes in the expression of some proteins were not statistically significant, mainly because data acquisition for label-free quantification was performed using the DDA mode, which collects thousands of peptides and compares them with the database and may yield false-positive results sometimes. PRM is used to detect specific proteins, and its sensitivity and accuracy are higher than LFQ, which may be attributed to insufficient sample size. Taken together, our findings indicate that Roxadustat might interfere with the content of differential proteins to exert

their pharmacological and/or toxicological effect in the urine of renal anemia patients.

3.3 Effect of Roxadustat on the urine metabolomics of patients

3.3.1 Classification of the metabolic profiles and differential metabolite identification. Urine samples were collected from 6 patients for metabolomics assays using LC-MS/MS. We compared total ion chromatograms (TIC) from the quality control (QC) samples in the positive or negative ion mode. As shown in Fig. 2A and B, the peak shape of the base peak chromatogram (BPC) was complete, and adjacent peaks were well separated from each other, indicating good repeatability and stability. This finding indicated that chromatographic and mass spectrometric conditions were suitable for sample identification. The PLS-DA score plot and OPLS-DA model showed a clear separation between the 2 groups (Fig. 2C and D), indicating that the urine metabolic states of renal anemia patients were significantly changed after Roxadustat treatment.

A VIP score > 1 and $P < 0.05$ was set as the criteria for differential metabolite screening. In total, 207 differential metabolites were identified, with 58 upregulated and 149 downregulated metabolites (ESI†). To further understand the
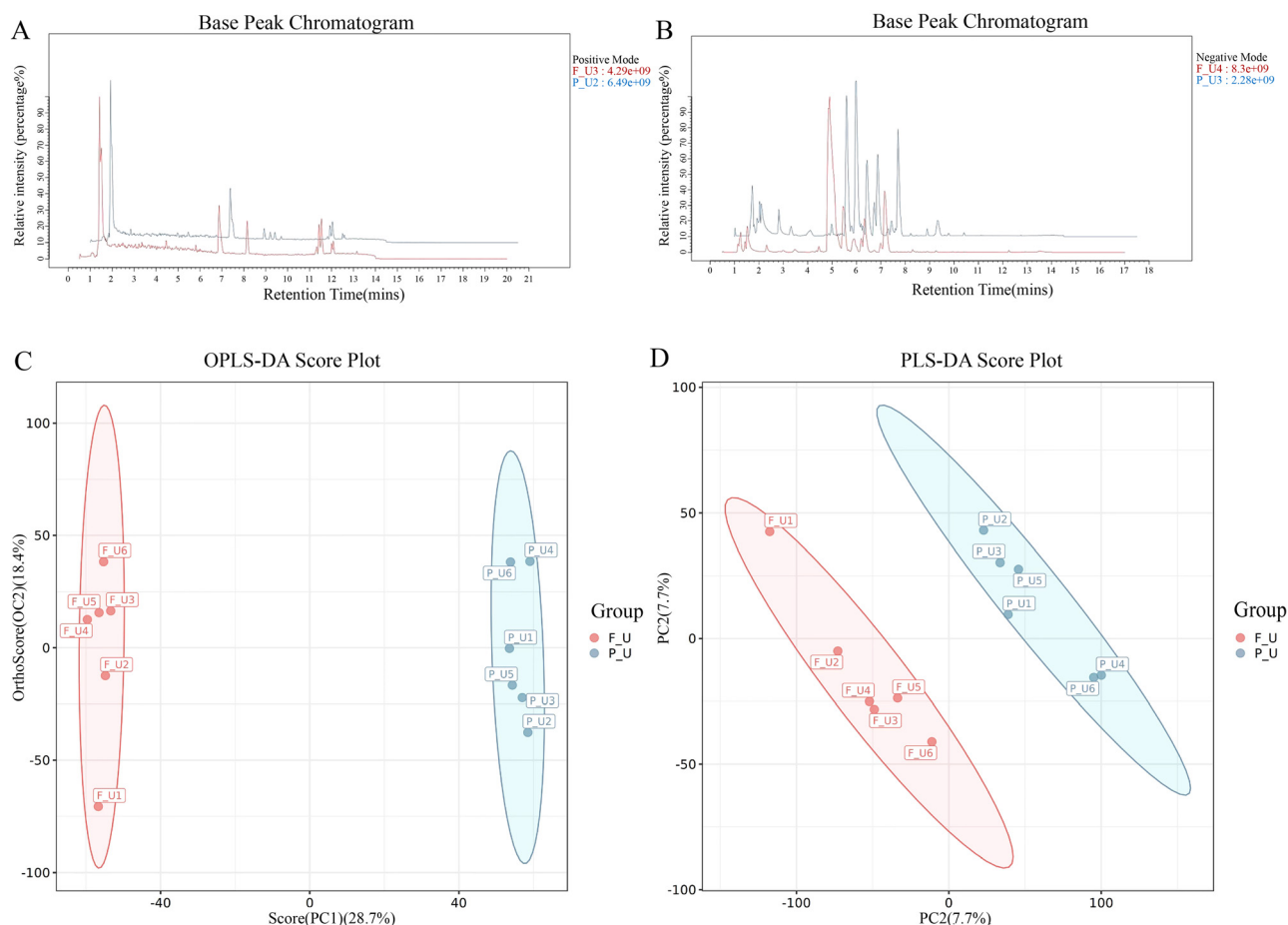

Fig. 2 The typical base peak intensity chromatograms: (A) positive ion mode; (B) negative ion mode. The OPLA-DA and PLS-DA score map of the quality control samples: (C) OPLA-DA score map; (D) PLS-DA score map.
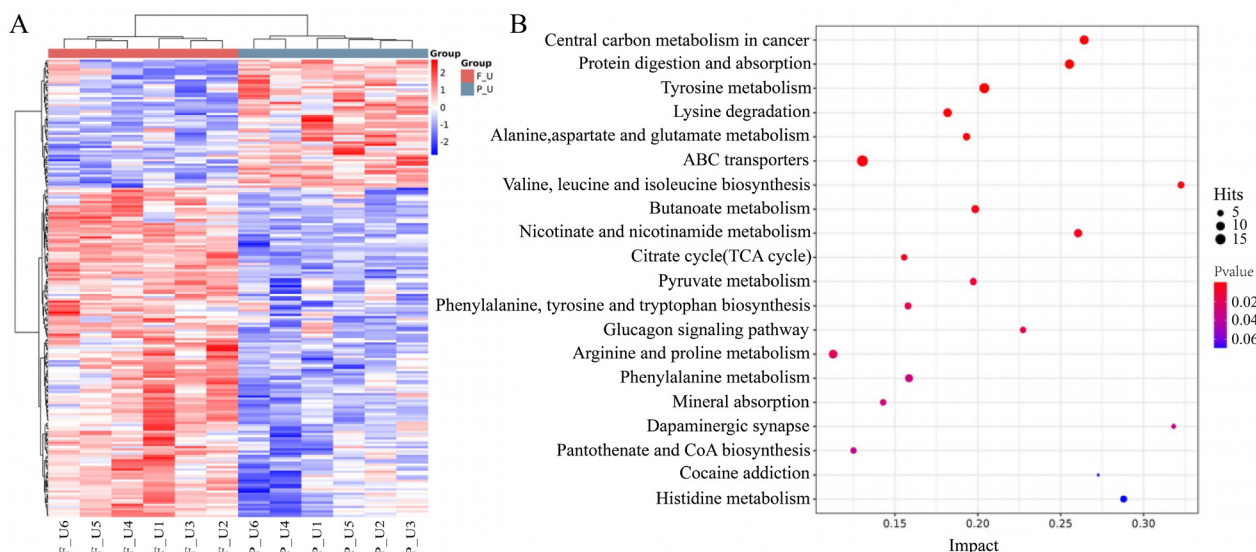
Fig. 3 Differential metabolites and their corresponding pathways. (A) Heatmap of the intensities of differential metabolites before and after medication. The degree of change is marked with different colours: red indicates upregulation, and blue represents downregulation. Each column represents an individual sample, and each row represents a metabolite. (B) The bubble chart of KEGG pathway enrichment.
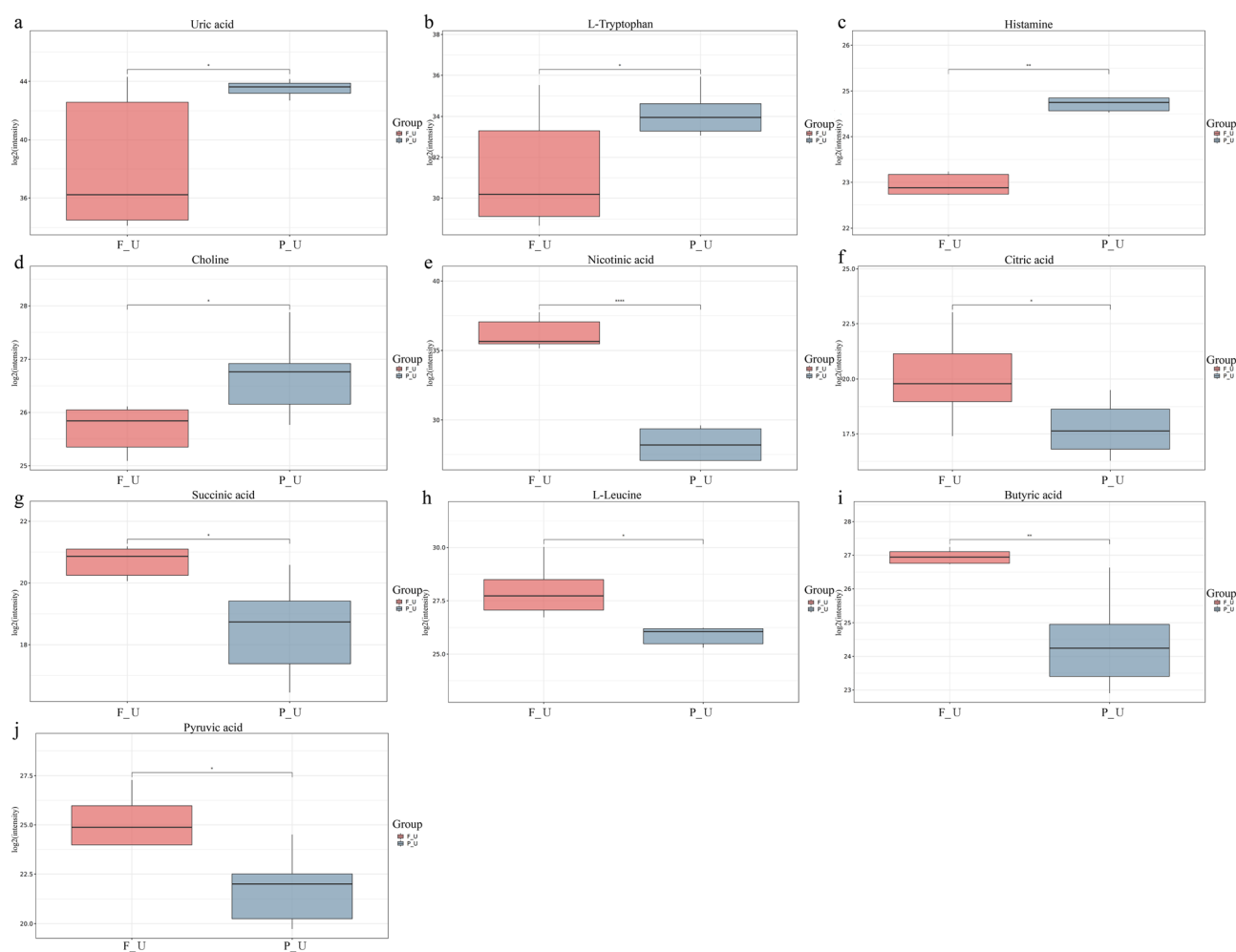

Fig. 4 The distribution of differences is visualized in a box plot. Each plot represents a different metabolite: (a) uric acid; (b) L-Tryptophan; (c) histamine; (d) choline; (e) nicotinic acid; (f) citric acid; (g) succinic acid; (h) L-Leucine; (i) butyric acid; (j) pyruvic acid.

metabolic changes, heatmaps were used to visualize the change after Roxadustat treatment (Fig. 3A). The significantly upregulated metabolites included uric acid, L-tryptophan, histamine, and choline. The significantly downregulated metabolites contained nicotinic acid, citric acid, succinic acid, L-leucine, butyric acid, and pyruvic acid (Fig. 4). KEGG analysis showed that these differentially expressed metabolites were significantly enriched in central carbon metabolism in cancer, protein digestion and absorption, valine, leucine and isoleucine biosynthesis, phenylalanine, tyrosine and tryptophan biosynthesis, the citrate cycle (TCA cycle), etc (Fig. 3B). These above-mentioned pathway alterations revealed that Roxadustat caused significant metabolite changes in the urine of renal anemia patients.

3.3.2 Pathway analysis based on differential metabolites. To uncover the most relevant biological pathways underlying Roxadustat's mechanism of action, ingenuity pathway analysis was performed by MetaboAnalyst (Metepa) (Fig. 5). The enrichment and topology analysis demonstrated that the mechanism of action was related to the metabolism of amino acids, including alanine, aspartate, glutamate, tyrosine, lysine, arginine, and proline.

3.4 Correlation analysis between proteomics and metabolomics

As stated above, we identified all differentially expressed proteins and metabolites and assessed their relationship by Spearman rank correlation analysis. The correlation coefficient is presented in a heatmap in ESI.† The high similarity between them was demonstrated by the cluster branches (the red colour indicates positive, and the blue colour means negative correlation). Spearman correlation analysis was conducted to screen significant differential proteins and metabolites with a Spearman correlation coefficient > 0.8 or < -0.8, and a co-expression network was generated. The network was visualized using Cytoscape software (ESI†). Then, we conducted KEGG pathway analysis of the differential proteins and metabolites to assess the potential relationship between differential proteins and differential metabolites (Fig. 6). It was found that the Ras signalling pathway, tryptophan metabolism, cholesterol metabolism, glycerophospholipid metabolism, and arginine and proline metabolism were significantly enriched.

4 Discussion

In the present study, using label-free quantitative proteomics and untargeted metabolomics, we identified the alterations in both proteins and metabolites that mediate the therapeutic effect of Roxadustat in renal anemia patients clinically. We identified 28 proteins and 207 metabolites that were significantly altered under Roxadustat treatment and are widely thought to be linked to lipid metabolism, kidney injury, and hypertension. To our knowledge, this is the first study investigating urine proteomics and metabolomics associated with Roxadustat.

4.1 The lipid-lowering effect of Roxadustat

As shown in ESI,† the NENF protein expression significantly increased after Roxadustat treatment. Studies on 3T3-L1 murine adipocytes showed that interference with the NENF gene significantly inhibited the mitogen-activated protein kinase (MAPK) pathway activation and promoted lipogenesis, suggesting that NENF is a potential negative regulator of early adipogenesis.[25] The above studies suggested that Roxadustat can suppress fat accumulation by upregulation of NENF expression. Moreover, Roxadustat may activate lipolysis by increasing IGFBP5 levels, which was validated with decreasing lipid levels in a previous study.[26] Our metabolomics analysis also demonstrated the lipid-lowering effect of FG-4572. Metabolomics-based investigations revealed that Roxadustat changed the levels of urine metabolites related to fat metabolism, such as quercetin and L-leucine. A previous study showed that quercetin transiently increased energy expenditure in mice,[27] and L-leucine was closely connected with energy balance.[28,29] Consistent with the literature, we found that "cholesterol metabolism (hsa04979)" and "glycerophospholipid metabolism (hsa00564)" were enriched during the integrated proteomics and metabolomics analysis. Taken together, our observations suggest that Roxadustat may regulate blood lipid levels by controlling the lipid metabolic pathways in renal anemia patients.

4.2 Renoprotective effect of Roxadustat

It is well-established that the inflammatory response is one of the key factors leading to kidney injury. In the present study, we found that after Roxadustat therapy, the significantly altered pathways in urine were those closely associated with
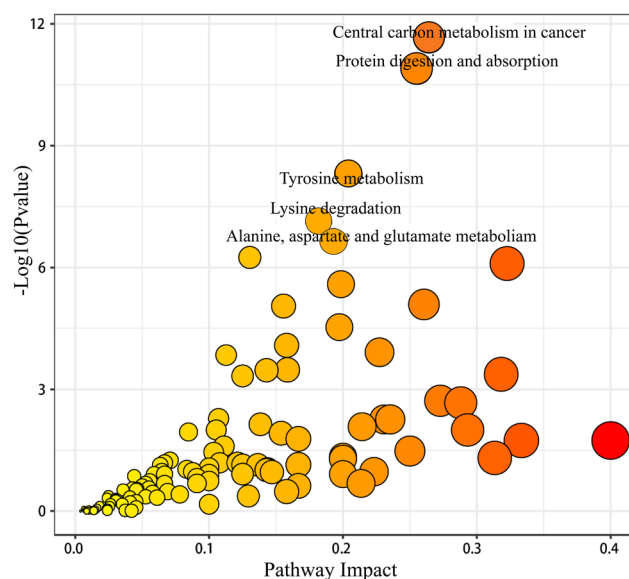

Fig. 5 The graph was obtained by plotting on the y-axis the $-\log$ of p-values from the pathway enrichment analysis and on the x-axis the pathway impact values derived from the pathway topology analysis. Colour intensity (white to red) reflects increasing statistical significance, while the circle diameter covaries with pathway impact.
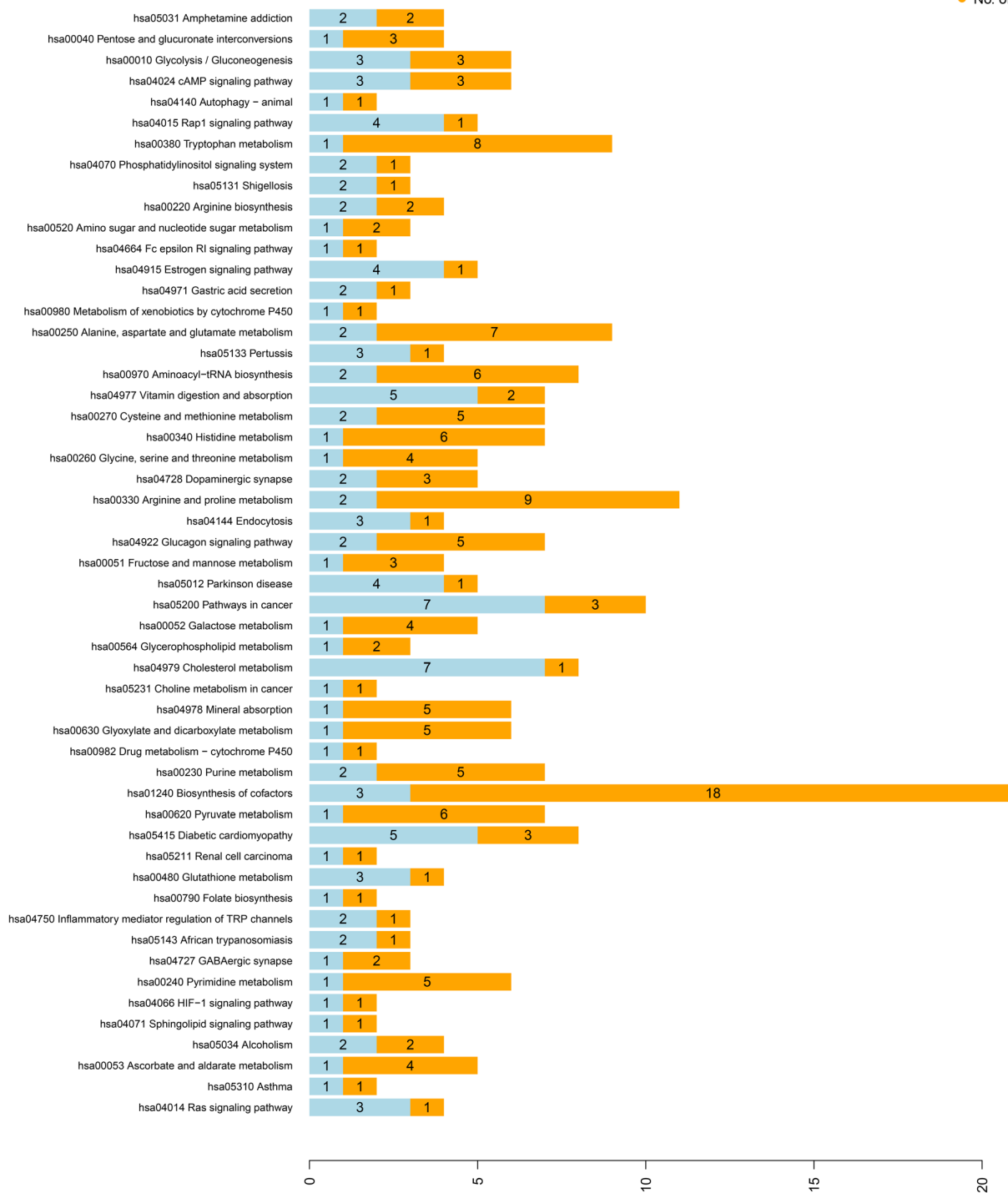
Fig. 6   KEGG pathway annotation of differential proteins and differential metabolites.

inflammation and oxidative stress. For instance, we found a significant decrease in succinic acid, an important intermediate of alanine, proline, and arginine metabolism and the TCA cycle involved in ROS generation in the mitochondria. Ample evidence suggests that treatment with sodium succinate could significantly decrease ROS levels and improve renal function.[30,31] Moreover, current evidence suggests that succinate acts as a metabolite in innate immune signalling to enhance inflammatory factors such as interleukin-1B *via* HIF-1α.[32] Therefore, it is highly conceivable that Roxadustat exerts its protective effects on chronic kidney disease by reducing succinic acid levels. Furthermore, based on previous studies and our metabolic screening, we speculate succinic may serve as a potential metabolite marker for excessive oxidative stress and inflammation-induced kidney damage.

Moreover, we found that arginine and proline metabolism networks were markedly altered. It has been shown that arginine is directly related to the production of nitric oxide in the body and participates in the regulation of end-stage renal degeneration.[30] Growing literature suggests that arginine is the only substrate for NO synthase with multiple functions in physiology,[33–35] including increasing the *in vivo* NO content, causing intrarenal vasodilation, improving hypoxia, increasing ATP supply, and improving renal tubular function. Similarly, we found that tryptophan and its derived metabolites increased after Roxadustat administration. Current evidence suggests that tryptophan levels are related to a rapid decline in eGFR,[36] suggesting that restoration of tryptophan metabolism may play an important role in Roxadustat's effects, and this hypothesis was confirmed and validated by our integrated proteomics and metabolomics analysis.

4.2 The antihypertensive effect of Roxadustat

Our integrated proteomics and metabolomics analysis found that the Ras signalling pathway (hsa04014) was significantly enriched after Roxadustat administration, consistent with the literature.[9] It is well-established that RAS signalling controls blood pressure (BP), body fluid balance, and tissue homeostasis.[37] Accordingly, dysregulation of RAS leads to BP elevation and plays a causative role in developing chronic kidney and cardiovascular disease.[38] Based on the above-mentioned theory, our study further corroborated that Roxadustat has huge prospects as a therapeutic target for hypertension associated with high RAS activity. Meanwhile, our study identified several proteins related to regulating blood vessel diameter after Roxadustat treatment, including CHGA, KLK1, and AGT, further suggesting that Roxadustat could directly control blood pressure levels by regulating the blood vessel diameter.

However, there were still some limitations in our study. First, the limited number of renal anemia patients, gender disbalance, and differences in the age range are the main factors that limit the generalizability of our findings. Moreover, the follow-up duration was limited and may affect the broad evaluation of the therapy outcomes. Therefore, more samples with long-term follow-up of Roxadustat treatment in CKD are needed. Besides, our findings are only preliminary; the universality and complexity of the HIF-1α pathway remain a huge challenge for investigators, warranting further research.

5 Conclusions

This is the first study of integrated proteomic and metabolomic analysis in the urine of patients with chronic kidney disease. We provide compelling evidence that Roxadustat plays a role in regulating blood lipid and blood pressure and protecting renal function by mediating protein expression and influencing metabolism.

List of abbreviations

HIF-PHI	Hypoxia-inducible factor prolyl hydroxylase inhibitor;
PHD	Prolyl hydroxylase domain
HIF	Hypoxia-inducible factors
EPO	Erythropoietin
RCTs	Randomized controlled trials
AKI	Acute kidney injury
TECs	Tubular epithelial cells
CKD	Chronic kidney disease
VSMCs	Vascular smooth muscle cells
MAP	Mean arterial pressure
Ang II	Angiotensin II
AGTR1	Angiotensin receptor type 1
PRM	Parallel reaction monitoring
TEAB	Triethylammonium bicarbonate
TFA	Trifluoroacetic acid
DDA	Data-dependent scan
AGC	The automatic gain control
GO	Gene ontology
KEGG	Kyoto Encyclopedia of Genes and Genomes
DIA	Data-independent acquisition
AGC	Automatic gain control
PCA	Principal component analysis
PLS-DA	Partial least-square discriminant analysis
OPLS-DA	Orthogonal partial least-square discriminant analysis
VIP	Variable importance on projection
FC	Fold change
SEM	Standard error of the mean
ACEI	Angiotensin-converting enzyme inhibitor
ARB	Angiotensin receptor blocker
DEPs	Differentially expressed proteins
TIC	Total ion chromatograms
QC	Quality control
BPC	Base peak chromatogram
MAPK	Mitogen-activated protein kinase.

Author contributions

Data curation: XY, RZ and LL; formal analysis: XY and HM; methodology: BG and LL; software: XY and BG; supervision: XZ; visualization: ZW; writing – original draft: XY and BG; writing – review & editing: XZ.

Data availability

The mass spectrometry proteomics data have been deposited to the PRIDE Archive (https://www.ebi.ac.uk/pride/archive/) *via* the PRIDE partner repository with the data set identifier PXD037002 (Project Webpage: https://www.ebi.ac.uk/pride/archive/projects/PXD037002, FTP Download: https://ftp.pride.ebi.ac.uk/pride/data/archive/2023/03/PXD037002). Metabolomics data have been deposited to the EMBL-EBI MetaboLights database (https://doi.org/10.1093/nar/gkz1019, PMID:31691833) with the identifier MTBLS7359.

Conflicts of interest

There are no conflicts to declare.

Acknowledgements

Notes and references

1 S. Dhillon, *Drugs*, 2019, **79**, 563–572.

2 Z. Yan and G. Xu, *Front. Med.*, 2020, **7**, 393.

3 Q. Zheng, H. Yang, X. Fu, Y. Huang, R. Wei, Y. Wang, Y. N. Liu and W. J. Liu, *Nephrol., Dial., Transplant.*, 2021, **36**, 1603–1615.

4 H. S. Ban, Y. Uto and H. Nakamura, *Expert Opin. Ther. Pat.*, 2021, **31**, 387–397.

5 K. Su, Z. Li, Y. Yu and X. Zhang, *Drug Discovery Today*, 2020, **25**, 1262–1269.

6 X. Zhang, Y. Zhang, P. Wang, S. Y. Zhang, Y. Dong, G. Zeng, Y. Yan, L. Sun, Q. Wu, H. Liu, B. Liu, W. Kong, X. Wang and C. Jiang, *Cell Metab.*, 2019, **30**(937–951), e935.

7 W. Li, A. Duan, Y. Xing, L. Xu and J. Yang, *Front. Cell Dev. Biol.*, 2021, **9**, 690079.

8 A. F. Miao, J. X. Liang, L. Yao, J. L. Han and L. J. Zhou, *Renal Failure*, 2021, **43**, 803–810.

9 J. Yu, S. Wang, W. Shi, W. Zhou, Y. Niu, S. Huang, Y. Zhang, A. Zhang and Z. Jia, *JCI Insight*, 2021, **6**(18), e133690.

10 N. Chen, C. Hao, X. Peng, H. Lin, A. Yin, L. Hao, Y. Tao, X. Liang, Z. Liu, C. Xing, J. Chen, L. Luo, L. Zuo, Y. Liao, B. C. Liu, R. Leong, C. Wang, C. Liu, T. Neff, L. Szczech and K. P. Yu, *N. Engl. J. Med.*, 2019, **381**, 1001–1010.

11 A. D. Nguyen, J. G. McDonald, R. K. Bruick and R. A. DeBose-Boyd, *J. Biol. Chem.*, 2007, **282**, 27436–27446.

12 Y. Yang, X. Yu, Y. Zhang, G. Ding, C. Zhu, S. Huang, Z. Jia and A. Zhang, *Clin. Sci.*, 2018, **132**, 825–838.

13 Q. Lin, S. Li, N. Jiang, H. Jin, X. Shao, X. Zhu, J. Wu, M. Zhang, Z. Zhang, J. Shen, W. Zhou, L. Gu, R. Lu and Z. Ni, *Autophagy*, 2020, 1–16, DOI: **10.1080/15548627.2020.1848971**.

14 M. Zhang, R. Dong, J. Yuan, J. Da, Y. Zha and Y. Long, *Clin. Exp. Pharmacol. Physiol.*, 2022, **49**, 311–318.

15 M. Wu, W. Chen, M. Miao, Q. Jin, S. Zhang, M. Bai, J. Fan, Y. Zhang, A. Zhang, Z. Jia and S. Huang, *Clin. Sci.*, 2021, **135**, 1707–1726.

16 Y. Huang, A. Di Lorenzo, W. Jiang, A. Cantalupo, W. C. Sessa and F. J. Giordano, *Hypertension*, 2013, **62**, 634–640.

17 D. P. Gale, S. K. Harten, C. D. Reid, E. G. Tuddenham and P. H. Maxwell, *Blood*, 2008, **112**, 919–921.

18 M. M. Hickey, T. Richardson, T. Wang, M. Mosqueira, E. Arguiri, H. Yu, Q. C. Yu, C. C. Solomides, E. E. Morrisey, T. S. Khurana, M. Christofidou-Solomidou and M. C. Simon, *J. Clin. Invest.*, 2010, **120**, 827–839.

19 R. F. Dubin and E. P. Rhee, *Clin. J. Am. Soc. Nephrol.*, 2020, **15**, 404–411.

20 J. Barratt and P. Topham, *Can. Med. Assoc. J.*, 2007, **177**, 361–368.

21 M. Cañadas-Garre, K. Anderson, J. McGoldrick, A. P. Maxwell and A. J. McKnight, *J. Proteomics*, 2019, **193**, 93–122.

22 V. Thongboonkerd, *Proteomics Clin Appl*, 2007, **1**, 780–791.

23 E. Zelena, W. B. Dunn, D. Broadhurst, S. Francis-McIntyre, K. M. Carroll, P. Begley, S. O'Hagan, J. D. Knowles, A. Halsall, I. D. Wilson and D. B. Kell, *Anal. Chem.*, 2009, **81**, 1357–1364.

24 E. J. Want, P. Masson, F. Michopoulos, I. D. Wilson, G. Theodoridis, R. S. Plumb, J. Shockcor, N. Loftus, E. Holmes and J. K. Nicholson, *Nat. Protoc.*, 2013, **8**, 17–32.

25 I. Kimura, M. Konishi, T. Asaki, N. Furukawa, K. Ukai, M. Mori, A. Hirasawa, G. Tsujimoto, M. Ohta, N. Itoh and M. Fujimoto, *Biochem. Biophys. Res. Commun.*, 2009, **381**, 75–80.

26 A. Xiang, G. Chu, Y. Zhu, G. Ma, G. Yang and S. Sun, *J. Cell Physiol.*, 2019, **234**(9), 15288–15298.

27 L. K. Stewart, J. L. Soileau, D. Ribnicky, Z. Q. Wang, I. Raskin, A. Poulev, M. Majewski, W. T. Cefalu and T. W. Gettys, *Metab., Clin. Exp.*, 2008, **57**, S39–46.

28 T. T. Zampieri, F. L. Torres-Leal, A. B. Campaña, F. B. Lima and J. Donato, *Nutrients*, 2014, **6**, 1364–1373.

29 Y. Zeng, T. Huang, N. Wang, Y. Xu, C. Sun, M. Huang, C. Chen, B. G. Oliver, C. Yi and H. Chen, *Front. Physiol.*, 2021, **12**, 700246.

30 S. P. Chapela, I. Burgos, C. Congost, R. Canzonieri, A. Muryan, M. Alonso and C. A. Stella, *Oxid. Med. Cell. Longevity*, 2018, **2018**, 1928945.

31 T. N. Andrienko, P. Pasdois, G. C. Pereira, M. J. Ovens and A. P. Halestrap, *J. Mol. Cell. Cardiol.*, 2017, **110**, 1–14.

32 G. M. Tannahill, A. M. Curtis, J. Adamik, E. M. Palsson-McDermott, A. F. McGettrick, G. Goel, C. Frezza, N. J. Bernard, B. Kelly, N. H. Foley, L. Zheng, A. Gardet, Z. Tong, S. S. Jany, S. C. Corr, M. Haneklaus, B. E. Caffrey, K. Pierce, S. Walmsley, F. C. Beasley, E. Cummins, V. Nizet, M. Whyte, C. T. Taylor, H. Lin, S. L. Masters, E. Gottlieb, V. P. Kelly, C. Clish, P. E. Auron, R. J. Xavier and L. A. O'Neill, *Nature*, 2013, **496**, 238–242.

33 A. Popolo, S. Adesso, A. Pinto, G. Autore and S. Marzocco, *Amino Acids*, 2014, **46**, 2271–2286.

34 B. Toczylowska, E. Zieminska, P. Senator and J. W. Lazarewicz, *Mol. Neurobiol.*, 2020, **57**, 3089–3105.

35 L. Gonzalez-Calero, M. Martin-Lorenzo, P. J. Martínez, M. Baldan-Martin, G. Ruiz-Hurtado, J. Segura, F. de la Cuesta, M. G. Barderas, L. M. Ruilope, F. Vivanco and G. Alvarez-Llamas, *Transl. Res.*, 2016, **178**, 25–37.e27.

36 C. A. Chou, C. N. Lin, D. T. Chiu, I. W. Chen and S. T. Chen, *J. Diabetes Invest.*, 2018, **9**, 366–374.

37 S. D. Crowley and T. M. Coffman, *Exp. Cell Res.*, 2012, **318**, 1049–1056.

38 S. B. Gurley, A. D. M. Riquier-Brison, J. Schnermann, M. A. Sparks, A. M. Allen, V. H. Haase, J. N. Snouwaert, T. H. Le, A. A. McDonough, B. H. Koller and T. M. Coffman, *Cell Metab.*, 2011, **13**, 469–475.